RSC Advances

PAPER

View Article Online
View Journal | View Issue

Cite this: *RSC Adv.*, 2020, **10**, 38695

Synthesis of novel calix[4]arene *p*-benzazole derivatives and investigation of their DNA binding and cleavage activities with molecular docking and experimental studies†

Seyda Cigdem Ozkan,[ab] Fatma Aksakal[c] and Aydan Yilmaz *[b]

In this study, novel *p*-benzimidazole-derived calix[4]arene compounds with different structures, and a benzothiazole-derived calix[4]arene compound, were synthesized by a microwave-assisted method and their structures were determined by FTIR, ^{1}H NMR, ^{13}C NMR, MALDI-TOF mass spectroscopy, and elemental analysis. The effects of functional calixarenes against bacterial (pBR322 plasmid DNA) and eukaryotic DNA (calf thymus DNA = CT-DNA) were investigated. The studies with plasmid DNA have shown that compounds **6** and **10** containing methyl and benzyl groups, respectively, have DNA cleavage activity at the highest concentrations (10 000 μM). Interactions with plasmid DNA using some restriction enzymes (*BamHI* and *HindIII*) were also investigated. The binding ability of *p*-substituted calix[4]arene compounds towards CT-DNA was examined using UV-vis and fluorescence spectroscopy and it was determined that some compounds showed efficiency. In particular, it was observed that the functional compounds (**10** and **5**) containing benzyl and chloro-groups had higher activity (K_b binding constants were found to be 7.1×10^3 M^{-1} and 9.3×10^2 M^{-1} respectively) on DNA than other compounds. Competitive binding experiments using ethidium bromide also gave an idea about the binding properties. Docking studies of the synthesized compounds with DNA were performed to predict the binding modes, affinities and noncovalent interactions stabilizing the DNA–compound complexes at the molecular level. Docking results were in good agreement with the experimental findings on the DNA binding activities of compounds. Based on these results, this preliminary study could shed light on future experimental antibacterial and/or anticancer research.

Received 31st August 2020
Accepted 14th September 2020

DOI: 10.1039/d0ra07486a

rsc.li/rsc-advances

Introduction

One of the developments in the field of chemistry in recent years has been the birth and progress of supramolecular chemistry. The discovery and many different features of macrostructures such as cyclodextrins,[1] crown ethers[2] and calixarenes[3] have contributed to the advancement in this area.

Calixarenes are excellent products of phenol-formaldehyde chemistry, which naturally act as sensors for many cations,[4] anions[5] and neutral molecules[6] due to their inherent structural properties. However, the idea that calixarenes can be used in areas such as medicine and biology has led scientists to work on this subject due to the increase in the occurrence of diseases (such as cancer, Alzheimer's, and Parkinson's) that cannot be completely cured and pose daily threats to human life. Various studies on biological applications of calixarenes, such as antibacterial,[7] antifungal,[8] antiviral,[9] anti-HIV,[10] anti-inflammatory,[11] anticancer,[12] and biotechnological studies,[13] have been carried out in recent years. Many studies on the interaction of calixarenes with DNA have been previously described;[14] DNA cleavage studies were performed using plasmid DNA, and highly effective results were obtained.[7b,15] However, there are also studies using eukaryotic DNA, and similar results have been obtained in these studies.[16]

Preliminary anticancer studies on interaction of candidate molecules with DNA are mostly examined. Most of the calixarene molecules that have been studied and those that bind to or interact with DNA are cationic structures.[12a,b,16b] However, as an alternative to these molecules, it is necessary to develop molecules that are uncharged but contain functional groups that can bind to DNA. For this purpose, the effects of calixarene compounds containing uncharged and functional groups on cancer cells were investigated and good results were obtained.[12c–e] In our study, we focus on synthesizing molecules that are uncharged but contain functional group(s) that can bind to

[a]*Department of Chemical and Chemical Processing Technologies, Acigol Vocational School of Technical Sciences, Nevsehir Haci Bektas Veli University, Nevsehir, Turkey. E-mail: aydan@selcuk.edu.tr; Fax: +90 332 2412499; Tel: +90 332 2233866*

[b]*Department of Chemistry, Faculty of Science, Selcuk University, 42075, Konya, Turkey*

[c]*Department of Chemistry, Faculty of Science, Hacettepe University, Ankara, Turkey*

† Electronic supplementary information (ESI) available. See DOI: 10.1039/d0ra07486a

DNA. We chose the benzimidazole groups and benzothiazole group, which have aromatic structures containing hetero groups as the functional groups.

The benzimidazole compounds are among the bioactive heterocyclic compounds, which exhibit a wide range of biological activities due to their imidazole nuclei.[17] In particular, functional benzimidazole derivatives have been synthesized as anticancer drugs in medicinal chemistry and their efficacy has been demonstrated by patents.[18] Benzimidazole compounds are fusion molecules, composed of the imidazole ring with a positive charge and a benzene ring with hydrophobic properties and a partial negative charge. Therefore, they are capable of interacting with both positive and negative regions of biological molecules. As is known, the DNA molecules have a partial negative charge due to the phosphate groups they contain, so the positive portions of the benzimidazole compounds tend to bind to DNA. There are a lot of studies on this topic and as a result, effective and remarkable data have been obtained and reported.[17]

In the literature, DNA binding modes include electrostatic interactions, intercalation interactions, binding to major and small grooves, and single-stranded DNA (ssDNA) base binding. Electrostatic interaction is the deterioration of the DNA charge balance due to interactions between the negatively charged phosphate backbone of DNA and the positively charged ends of the molecules.[18] Intercalation occurs when an aromatic planar substituent is inserted between the DNA base pairs causing the unwinding and lengthening of the DNA helix.[19] Groove binding is caused by groove binders connected to the major or minor grooves of the DNA. This involves hydrogen bonding or van der Waals interactions of the molecule with the nucleic acid without substantially disrupting the duplex structure, or bases, as opposed to intercalation.[20] ssDNA base binding results from binding to the single-stranded DNA of some proteins.[21]

In this study, we report the synthesis and characterization of new *p-tert*-butylcalix[4]arenes with benzimidazole derivatives and a benzothiazole derivative. The DNA cleavage effects of the synthesized compounds were investigated using pBR322 plasmid DNA by the agarose gel electrophoresis method. The determination of the site of DNA cleavage with *BamHI* and *HindIII* restriction enzymes was carried out for all compounds. In another study, the effects of synthesized calixarene compounds against CT-DNA were investigated using fluorescence and UV-vis. spectrometry. Binding constants (K_b) and quenching constants (K_{sv}) were calculated for some compounds that were effective in fluorescence spectrometry. Finally, competitive binding experiments with ethidium bromide were performed and quenching constants (K_{sv}) were determined. To support the experimental results with theoretical studies, molecular docking studies of the synthesized compounds with the DNA were also performed.

Results and discussion

Synthesis of *p*-benzazole derivatives of calix[4]arenes

The starting compound, *p-tert*-butylcalix[4]arene (**1**) and derivative compounds **2** and **3** were synthesized according to the literature procedures (Scheme 1).[22–24]

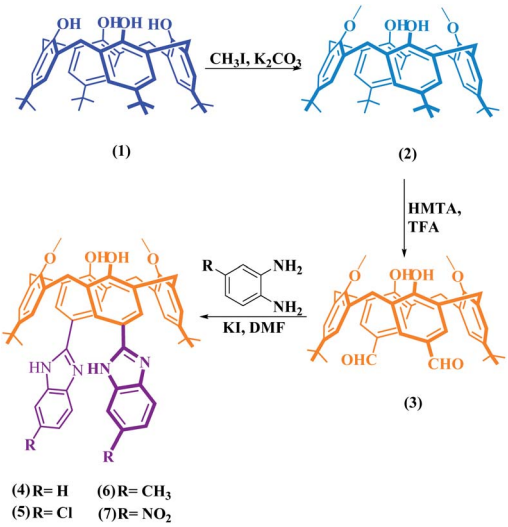

Scheme 1 Schematic route for the synthesis of *p*-benzimidazole derivatives of calix[4]arenes.

To obtain benzimidazole compounds that have different structures, the dialdehyde-derived calix[4]arene compound **3** was reacted with *o*-phenylenediamine and its 4-substituted derivatives separately in the presence of KI in DMF (Scheme 1). Before the mixtures were boiled in a domestic microwave oven for a few minutes, they were heated at 80 °C under a reflux condenser. The reactions were monitored by thin-layer chromatography (TLC). After purification, the FTIR spectrum showed that the peak at 1680 cm^{-1} of the aldehyde carbonyl was completely gone and the peaks belonging to the benzimidazole group (approximately 1660 cm^{-1} and 1620 cm^{-1}) were formed. Also, –NH protons belonging to the benzimidazole group were determined by ^{1}H NMR at 12.54 ppm for compound **4**, 12.76 ppm for compound **5**, 12.80 ppm for compound **6**, and 13.30 ppm for compound **7**; NH protons were in resonance. The confirmations of the cone conformations of the compounds obtained were carried out by ^{1}H NMR to give the following results for $ArCH_2Ar$ protons: compound **4** had a doublet pair at 3.57 ppm and 4.24 ppm $J = 13.1$ Hz; compound **5** had a doublet pair at 3.61 ppm and 4.27 ppm, $J = 12.8$ Hz; compound **6** had a doublet pair at 3.60 ppm and 4.28 ppm, $J = 12.8$ Hz; compound **7** had a doublet pair at 3.60 ppm and 4.26 ppm, $J = 13.1$ Hz. The characterizations of the synthesized compounds were supported by ^{13}C NMR and MALDI TOF MS analyses (Fig. S1 and S2†).

In the second part of the synthesis, to obtain *N*-substituted benzimidazole derivatives, *o*-phenylenediamine was reacted with benzyl bromide and *p*-nitrobenzyl bromide and converted into *N*-substituted *o*-phenylenediamine derivatives (**8** and **9**) (Scheme 2) as in the literature,[25] and the structural analyses were performed using FTIR and ^{1}H NMR. The obtained compounds were reacted with dialdehyde-derived calixarene (**3**) and compounds **10** and **11** were synthesized. In the FTIR analysis of these compounds, the peak of the aldehyde group disappeared and the benzimidazole imine peak was formed; ^{1}H NMR spectra were also determined. The confirmations of the

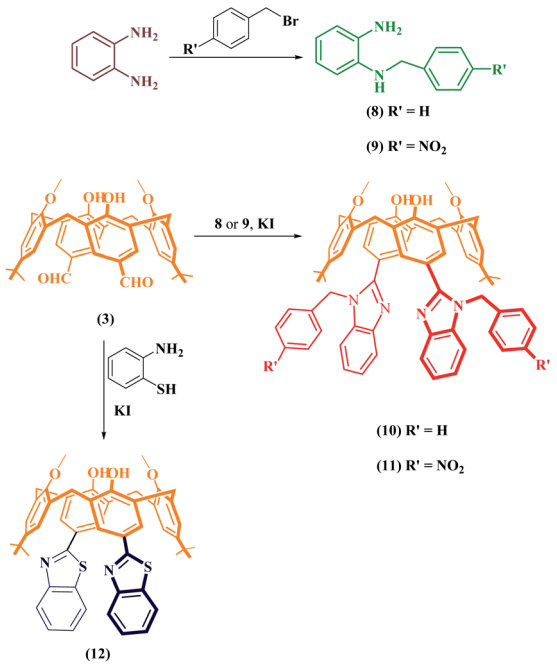

Scheme 2 Schematic route for the synthesis of functional *p*-benzimidazole derivatives and a benzothiazole derivative of calix[4]arenes.

cone conformations of the compounds were again provided by ^{1}H NMR analysis. For the synthesis of the benzothiazole derivative of calixarene (**12**), the synthetic pathway is given in Scheme 2. Compound **3** and 2-aminothiophenol were heated in the presence of KI in DMF by using the synthesis-type microwave oven for 3 hours and compound **12** was obtained. Structure analysis was performed by FTIR and ^{1}H NMR. In the FTIR spectrum of this compound, the carbonyl band of the aldehyde group disappeared while the imine band appeared at 1658 cm^{-1}. In the ^{1}H NMR spectrum, ArCH$_2$Ar protons were exposed as 3.57 ppm and 4.36 ppm as a doublet pair (J = 13.3 Hz). ^{13}C NMR and MALDI-TOF MS analyses were performed for all compounds and their structures were illuminated (Fig. S3 and S4†).

DNA cleavage studies with pBR322 plasmid DNA

Plasmid DNAs are fragments of protective DNA that are contained within the bacterial cell that can copy itself, apart from the chromosomal DNA of the bacterium. When bacteria are exposed to any external agent (various chemicals *etc.*), they use their DNA to protect themselves. Therefore, molecules that can damage or break down the plasmid DNA cause the bacteria to die by preventing their growth. For all these reasons, we investigated the activity of the synthesized molecules on this DNA using the pBR322 plasmid DNA. These studies were carried out with the aim of pioneering DNA studies, presenting the first ideas about the interaction of compounds with DNA.

The interactions of synthesized calixarene compounds with supercoiled pBR322 DNA were investigated using agarose gel electrophoresis. When circular plasmid DNA is subjected to electrophoresis, the fastest migrating supercoiled Form I, the slower-moving open circular Form II, and the linear Form III will all be generated, with migration in between.[26]

Firstly, in order to determine whether dimethylformamide (DMF) as a solvent in the various concentrations of the compound samples affected pBR322 plasmid DNA, incubation with plasmid DNA for the purpose of control in the same proportions was performed using the same conditions. According to the obtained results, the solvent had little effect on the plasmid DNA (Fig. 1a). According to the electrophoresis image seen in Fig. 1a, compound **4** is not effective on the plasmid DNA at all the studied concentrations. In the embodiment of Fig. 1b, compound **5** destroyed the Form II (open circular form) structure that was present in the plasmid DNA at the first three concentrations. However, the Form I (supercoiled form) structure remained. In the same image, for compound **6** on the right side of the gel, all bands of plasmid DNA (Form I and Form II) at the maximum concentration of 10 000 μM disappeared, while the Form I structure was formed in more dilute concentrations, and the Form II structure was observed as very slim at the low concentration. We can say that this compound showed the cleavage effect on plasmid DNA at this concentration.[7b]

The image on the left (column 2–5) of Fig. 2a shows the interaction of the pBR322 plasmid DNA with compound **7**. Accordingly, at all concentrations of this compound, a higher band was observed showing that the molecular weight of the Form I structure (supercoiled) was increased. A similar situation was observed in the 100% DMF sample used for the control, but a band closer to Form I was observed below. From this, we can say that compound **7** decreases the mobility and density of the Form I structure. Similarly, results were obtained in the literature where functional calixarene molecules reduced the mobility of the Form I structure of plasmid DNA.[7b,15] Calixarene molecules, which are large in structure, can bind to the supercoiled structure of DNA and limit its mobility. The same image (Fig. 2a) on the right side (column 6–9) shows the interaction of compound **11** with pBR322 plasmid DNA. According to this, at the highest concentration of this compound (**11**), the supercoiled DNA fragment (Form I) and the open circular form (Form II) are broken and are, therefore, converted into smaller DNA fragments. At the lower concentrations, the Form I band was

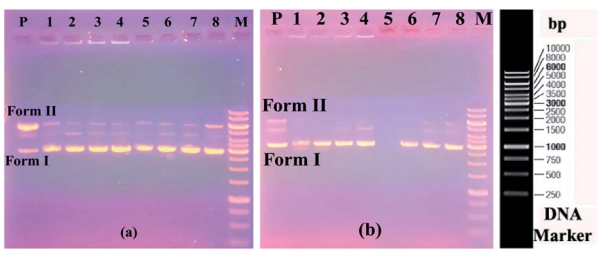

Fig. 1 Electrophoresis images of pBR322 plasmid DNA interacting with compounds. P: only plasmid DNA, M: DNA marker. (a) Compound **4**, 1→4: 10 000 μM, 5000 μM, 2500 μM, 1250 μM; 5→8: only solvent (DMF) 100%, 50%, 25% and 12.5%. (b) Compound **5**, 1→4: 10 000 μM, 5000 μM, 2500 μM, 1250 μM; compound **6**, 5→8: 10 000 μM, 5000 μM, 2500 μM, 1250 μM. (c) Standard DNA marker (1 Kb DNA ladder).

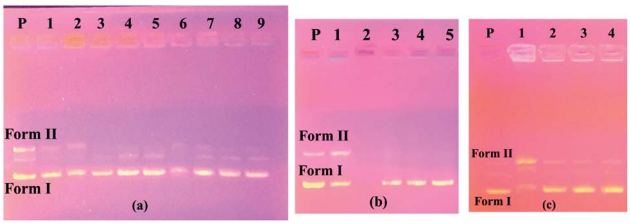

Fig. 2 Electrophoresis images of pBR322 plasmid DNA interacting with compounds. P: only plasmid DNA. (a) 1: DMF control (100%), compound **7**, 2→5: 10 000 μM, 5000 μM, 2500 μM, 1250 μM; compound **11**, 6→9: 10 000 μM, 5000 μM, 2500 μM, 1250 μM. (b) Compound **10**, 1: DMF control (100%), 2→5: 10 000 μM, 5000 μM, 2500 μM, 1250 μM. (c) Compound **12**, 1→4: 10 000 μM, 5000 μM, 2500 μM, 1250 μM.

observed, albeit higher. In the electrophoresis image shown in Fig. 2b (column 2–5) is the interaction of compound **10** with plasmid DNA. Accordingly, all bands of the plasmid DNA (Form I and Form II) at the highest concentration (10 000 μM) disappeared. A cleavage effect was observed at this concentration.[7b] Form I structure was observed at lower concentrations. On the other hand, the Form II structure was not observed. Fig. 2c shows the interaction of plasmid DNA with compound **12** on the left side (column 1–4) of the electrophoresis image. At the highest concentration of this compound, both the density and the mobility of the supercoiled Form I structure of the plasmid DNA decreased. On the other hand, the density of the open circular structure, Form II, increased. At lower concentrations, the bands appeared as in the control plasmid.

According to the obtained results, the two most effective compounds were compounds **6** and **10**, which have methyl and benzyl groups, respectively. The benzyl group has a rigid and planar structure due to the benzene ring it contains. Therefore, it was expected that compound **10** would approach the aromatic core bases of DNA. Unlike other benzimidazole compounds, the methyl group in compound **6** may bind hydrophobically to DNA due to its hydrophobic properties, as reported studies in the literature.[37,38]

In the second part of the study, to determine the ability of the synthesized heterocyclic *p-tert*-butylcalix[4]arene derivatives to cleave DNA molecules at the positions at which particular short sequences of bases are present, we used *BamHI* and *HindIII* enzymes. Restriction endonuclease analyses of compound-pBR322 plasmid DNA inserts were performed using these enzymes. *BamHI* and *HindIII* enzymes cut DNA at specific sequences as follows: 5′-G/GATCC-3′ and 5′-A/AGCTT-3′. As a result of the cutting process, Form I (supercoiled form) DNA and Form II (nicked form) DNA constructs were converted into Form III DNA in linear form.

Fig. 3a shows the results of the experiment with the *BamHI* enzyme. On the right side of the figure, it was found that the *BamHI* enzyme cut the plasmid DNA at all concentrations of compound **4**. The electropherograms on the left side of the same figure were formed by the control samples made as a control.

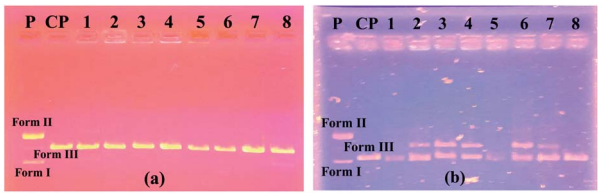

Fig. 3 Electrophoresis images of compound-pBR322 plasmid DNA mixture after interactions with the enzymes *BamHI* (a) and *HindIII* (b). P: plasmid DNA, CP: cut plasmid DNA, 1→4: only solvent (DMF) 100%, 50%, 25%, 12.5%; compound **4**, 5→8: 10 000 μM, 5000 μM, 2500 μM, 1250 μM.

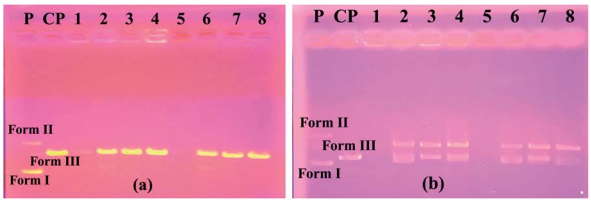

Fig. 4 Electrophoresis images of compound-pBR322 plasmid DNA mixture after interactions with the enzymes *BamHI* (a) and *HindIII* (b). P: plasmid DNA, CP: cut plasmid DNA, compound **5**, 1→4: 10 000 μM, 5000 μM, 2500 μM, 1250 μM; compound **6**, 5→8: 10 000 μM, 5000 μM, 2500 μM, 1250 μM.

Accordingly, the enzyme made the cuts in the highest DMF ratios. In Fig. 3b, a gel image of the *HindIII* segment is shown. On the right side of this figure, the enzyme cuts the plasmid DNA at all concentrations of compound **4**. On the left side of the same figure, the enzyme again cuts in the samples containing only the solvent.

At the highest concentration of compound **5** on the left side of Fig. 4a, it was observed that plasmid DNA was almost absent and the linear Form III structure had very low density and *BamHI* enzyme was cut at lower concentrations of this compound. On the right side of the same figure, plasmid DNA was not seen at the first high concentration of compound **5** and the *BamHI* enzyme was cut at lower concentrations. In Fig. 4b, the gel image of the *HindIII* segment is given. From the figure, it is seen that at the highest concentrations of compounds **5** and **6** do not have visible plasmid DNA bands (columns 1 and 5), whereas, at lower concentrations of these compounds, the enzyme cut the plasmid DNA.

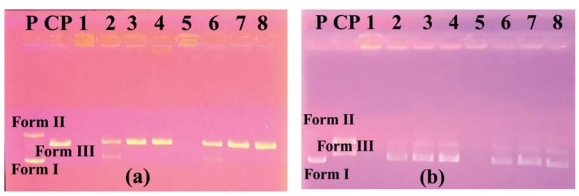

Fig. 5 Electrophoresis images of compound-pBR322 plasmid DNA mixture after interactions with the enzymes *BamHI* (a) and *HindIII* (b). P: plasmid DNA, CP: cut plasmid DNA, compound **7**, 1→4: 10 000 μM, 5000 μM, 2500 μM, 1250 μM; compound **11**, 5→8: 10 000 μM, 5000 μM, 2500 μM, 1250 μM.

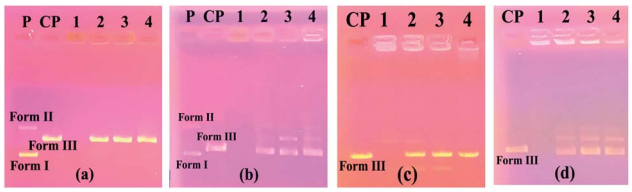

Fig. 6 Electrophoresis images of the compound-pBR322 plasmid DNA mixture after interaction with the enzymes *BamHI* (a and c) and *HindIII* (b and d), (a and b). P: plasmid DNA, CP: cut plasmid DNA, compound **10**, 1→4: 10 000–1250 μM; (c and d) compound **12**, 1→4: 10 000–1250 μM.

In Fig. 5a, it was found that plasmid DNA did not appear in both compounds **7** and **11** at the first high concentrations, whereas in lower concentrations, the *BamHI* enzyme cut the plasmid DNA. The *HindIII* enzyme cut image in Fig. 5b shows that there are no plasmid DNA bands at the highest concentrations of both compounds **7** and **11**, while the enzyme cut the plasmid DNA partially at the lower concentrations of these compounds.

Fig. 6a and c show the results of the experiments with compound **10** and compound **12** of the *BamHI* enzyme, respectively. At the first high concentration of both compounds, all the bands of plasmid DNA were not found whereas, at lower concentrations of these compounds, the *BamHI* enzyme cut the plasmid DNA. Similar results were observed in the experimental results with the *HindIII* enzyme (Fig. 6b and d).

The obtained results showed that the compounds had no interest in the specific binding regions of the enzymes.

DNA interaction studies with calf thymus DNA

DNA-binding studies by UV-vis absorption spectroscopy. UV-vis spectroscopy is one of the basic and useful tools that give an idea about whether the compound or substance interacts with calf thymus DNA (CT-DNA) or its ability to bind. CT-DNA gives a band at 258–260 nm, resulting from the π–π* transitions between the base pairs of DNA. When the concentration of the compound or the substance is kept constant and the concentration of DNA is regularly increased, the increase or decrease in the absorption of DNA is one of the proofs that the interaction has occurred. These interactions may be the distortion of the hydrogen bond between the base pairs, covalent bonding or intercalation. On the other hand, following the absorption of the compound/compounds is another method used for investigating compound–DNA interactions.

In this study, we also followed the absorbances of the compounds (**4–7** and **10–12**). Upon the addition of increasing amounts of CT-DNA, a significant hyperchromism was observed for all compounds except compound **7** (Fig. 7).[26] In the absorption spectrum of compound **7**, a partial increase in electronic absorption (at 396 nm) was observed with the increase in the DNA concentration as in other compounds; however, the graph was not included here because the increase remained low as compared to other compounds.

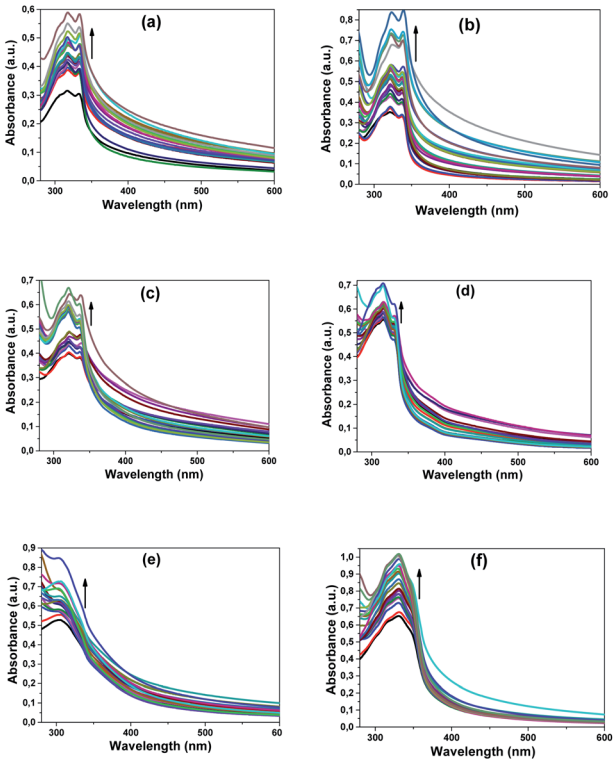

Fig. 7 The obtained UV-vis absorption spectra of the compounds on adding CT-DNA in increasing concentrations (from bottom to top (0–50 μM)) in increments of 2.5 μM of CT-DNA, additionally 75 μM and 100 μM CT-DNA. (a) Compound **4**, (b) compound **5**, (c) compound **6**, (d) Compound **10**, (e) compound **11**, (f) compound **12**. The arrows show the changes upon increasing the amounts of CT-DNA.

As shown in Fig. 7, there was a regular increase in the absorbance of compound **4** at 318 and 333 nm, compound **5** at 322 and 338 nm, and compound **6** at 317 and 320 nm on increasing the CT-DNA concentration. Likewise, a steady increase in CT-DNA concentration was observed with the absorbances of compound **10** at 316 and 330 nm, compound **11** at 304 nm and compound **12** at 330 nm. When the all spectra were examined, it was observed that there was no shift in wavelengths and only the intensity of absorption increased.

Although there were no appreciable changes in the absorption spectra of the compounds, the positions of the intra-compound bands were observed, and a strong chromic effect was observed with increased CT-DNA concentration. This observed change shows that the compounds most likely interacted with DNA in the groove binding mode.[27a–c] This observed hyperchromism may have occurred as a result of external contact, such as surface bonding with the DNA double-strand.[27a] This surface contact may have occurred as a result of hydrogen bonding, electrostatic interactions, or π-interactions between aromatic groups. The compounds that contain imidazole groups, other functional groups (such as Cl, NO_2, or methyl) and aromatic rings can cause these conditions.

Based on these results, we can say or suggest that the compounds most likely bind to CT-DNA. However, extra studies were needed to obtain accurate and reliable results and to

determine the mode of binding of the compounds with CT-DNA; hence, fluorimetry and competitive binding studies with EtBr, known as an intercalator, were performed to clarify the DNA-binding mode.

DNA-binding studies by fluorescence spectroscopy. All the compounds showed fluorescence properties and exhibited good fluorescence, except compound **7**. Since the fluorescence intensity of compound **7** was very low, experimental evaluation could not be performed. Interestingly, the fluorescence intensity of compound **6** did not change on adding CT-DNA; as such, the spectra are not shown herein. The monitoring of fluorescence intensities by the addition of CT-DNA was performed only for the compounds that gave emission spectra. The concentrations of the compounds were kept constant at 25 μM; changes in the emission spectra of the compounds were recorded on adding CT-DNA up to 50 μM, with increments of 2.5 or 5 μM, and also at concentrations of 75 μM and 100 μM. Due to the high emission intensities, compounds **4** and **5** were studied at 10 μM. While working with these compounds (**4** and **5**), CT-DNA was increased to a maximum of 30 μM in increments of 5 μM. It was concluded that the compounds interacted with DNA or bound to DNA in the event of a decrease or increase in the emission spectra of the compounds. As a result of the computational processes, taking the effects into account, DNA binding constants or extinguishing constants were calculated.[28]

The quantitative estimation of extinguishing experiments in terms of the binding constant was conducted using the following Stern–Volmer equation:[28]

$$F_0/F = 1 + K_{sv}[Q]$$

F_0 and F are the fluorescence intensities of the compounds in the absence and presence of CT-DNA, respectively. K_{sv} is the linear Stern–Volmer quenching constant and [Q] is the concentration of CT-DNA.

Another modified Stern–Volmer equation was used to calculate the DNA binding constants of the compounds from both the increase and decrease in emission intensities:[28]

$$\log(F_0 - F)/F = \log K_b + n \log[DNA]$$

F_0 and F are the fluorescence intensities of the compounds in the absence and presence of DNA, respectively, K_b is the binding constant, n is the number of binding sites of the compound to CT-DNA, and [DNA] is the concentration of DNA in base pairs.

An increase in the emission intensity of compound **4** at 401 nm was observed with increasing DNA concentration according to the emission spectrum obtained using 330 nm excitation (Fig. 8a). The binding constant K_b was determined from the plot of $\log(F_0 - F)/F$ *vs.* log[DNA] and was found to be 8.6×10^2 M^{-1} (Fig. 8b). A regular increase in the emission intensity of compound **5** at 431 nm was observed with increasing the DNA concentration; the emission maximum wavelength of this compound shifted slightly (1 nm) (Fig. 9a). The K_b constant calculated from the linear graph obtained was 9.3×10^2 M^{-1} (Fig. 9b).

The fluorescence spectra obtained using the excitation wavelength at 300 nm for compound **10** are shown in Fig. 10a. When we look at the fluorescence spectrum of compound **10**, it can be said that a different state occurred. A slight decrease in fluorescence the intensity was observed with the addition of DNA. The quenching constant K_{sv} 9.8×10^3 M^{-1} was calculated from the fluorescence quenching measurement at 381 nm

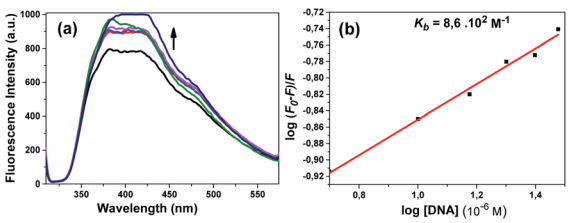

Fig. 8 Fluorescence spectra obtained by adding CT-DNA in increasing concentrations (from bottom to top (0–30 μM)) with increments of 5 μM of CT-DNA of compound **4** (a); the linear graph from which the K_b constant was calculated (b). The arrow shows the changes upon increasing the amounts of CT-DNA.

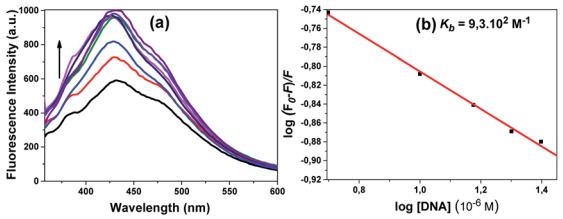

Fig. 9 Fluorescence spectra obtained by adding CT-DNA in increasing concentrations (from bottom to top (0–30 μM) with increments of 5 μM of CT-DNA, additionally 75 μM and 100 μM CT-DNA) of compound **5** (a); the linear graph from which the K_b constant was calculated (b). The arrow shows the changes upon increasing the amounts of CT-DNA.

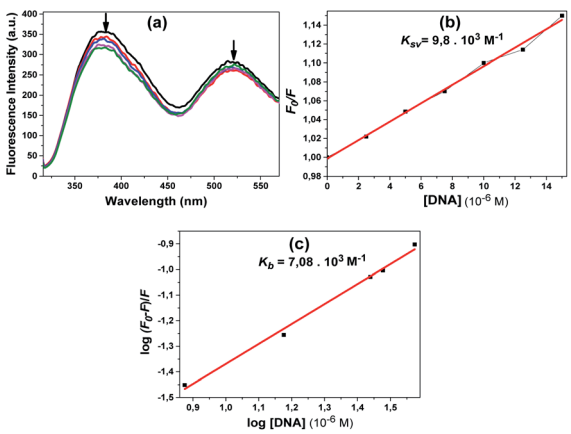

Fig. 10 Fluorescence spectra obtained by adding CT-DNA in increasing concentrations [from bottom to top (0–50 μM) with increments of 2.5 μM of CT-DNA and additionally, 75 μM and 100 μM CT-DNA] of compound **10** (a); the linear graph from which the K_b constant was calculated (b); the linear graph from which the K_b constant was calculated (c). The arrows show the changes upon increasing the amounts of CT-DNA.

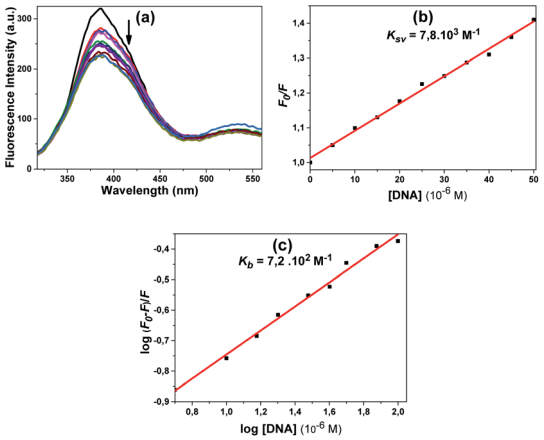

Fig. 11 Fluorescence spectra obtained by adding CT-DNA in increasing concentrations (from bottom to top (0–50 μM)) with increments of 5 μM of CT-DNA of compound **11** (a); the linear graph from which the K_{sv} constant was calculated (b); the linear graph from which the K_b constant was calculated (c). The arrow shows the changes upon increasing the amounts of CT-DNA.

(Fig. 10b). The calculated K_b constant from the linear graph obtained was 7.1 × 10^3 M^{-1} (Fig. 10c).

Compound **11** also showed a result similar to compound **10**; the fluorescence spectra obtained using the excitation wavelength at 300 nm are shown in Fig. 11a. A slight decrease in fluorescence intensity was observed with the addition of DNA. The quenching constant K_{sv} 7.8 × 10^3 M^{-1} was calculated from the fluorescence quenching measurement at 386 nm (Fig. 11b).

Fig. 12a shows the fluorescence spectra obtained at the excitation wavelength of 300 nm for **12**. With increasing DNA concentration, the emission band of the compound at 384 nm showed a steady decrease (Fig. 12a). The quenching constant

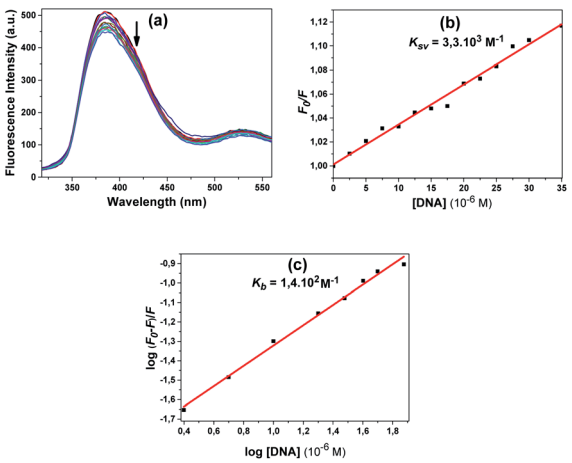

Fig. 12 Fluorescence spectra obtained by adding CT-DNA in increasing concentrations (from bottom to top (0–50 μM) with increments of 2.5 μM of CT-DNA and additionally, 75 μM and 100 μM CT-DNA) of compound **12** (a); the linear graph from which the K_{sv} constant was calculated (b); the linear graph from which the K_b constant was calculated (c). The arrow shows the changes upon increasing the amounts of CT-DNA.

Table 1 The calculated quenching (K_{sv}) and binding constants (K_b) (M^{-1}), the number of binding sites of the compound to CT-DNA (n), and correlation coefficient values (R^2) of the compounds that interact with DNA

A[a]	B[b]	K_b	n	K_{sv}	R^2
4	—	8.6 × 10^2	0.37	—	0.991
5	Chloro	9.3 × 10^2	0.45	—	0.996
10	Benzyl	7.1 × 10^3	0.78	9.8 × 10^3	0.991/0.993[c]
11	*p*-Nitro benzyl	7.2 × 10^2	0.39	7.8 × 10^3	0.99/0.993[c]
12	Sulfur (S)	1.4 × 10^2	0.52	3.3 × 10^3	0.993/0.989[c]

[a] Compound. [b] Functional Group. [c] R^2 values are given for K_b and K_{sv} constants, respectively.

K_{sv}, 3.3 × 10^3 M^{-1}, was calculated using the Stern–Volmer equation (Fig. 12b).

According to the obtained results, the fluorescence intensities of some of the compounds increased with the addition of CT-DNA while others decreased. The compounds that had decreased fluorescence intensities were compounds **10**, **11** and **12**. The compounds that had increased emission intensities were compounds **4** and **5**. The calculated mathematical data are given in Table 1. According to these results, the compound that had the highest binding constant was **10**. DNA binding strength ranking was **5** > **4** > **11** > **12**. The quenching constants were also calculated from here, as the emission intensity of the compounds decreased with increasing DNA concentration for compounds **4**, **5** and **12**. The found K_{sv} constants are compatible with the results in the K_b binding constants. The numbers n found for all compounds are approximately equal to one, indicating that the compounds bind 1 : 1 with DNA. Both results showed that the functional calixarene compounds interacted by binding to CT-DNA.

Competitive binding experiments in the presence of ethidium bromide

One of the useful experimental methods for understanding whether the compounds interact with CT-DNA is to monitor the fluorescence intensity of the EtBr–DNA complex using ethidium bromide (EtBr). EtBr is one of the most sensitive fluorescent probes due to its planar structure and is connected to the DNA by the intercalative mode.[29] When the fluorescence spectrum in EtBr alone is taken up, an emission peak at about 600 nm is observed and its intensity is very low due to the solvent action.[29] However, when CT-DNA is added to the environment, the emission intensity of EtBr increases due to the formed EtBr + DNA complex.[29] If there is a substance that binds to DNA in the environment, the fluorescence intensity of the EtBr–DNA complex decreases[29] because the substance inhibits EtBr interaction with DNA. From the resulting decrease, Stern–Volmer quenching constants[28] can be calculated and the binding strength of molecules or substances to DNA can be compared.

For these experiments, the CT-DNA + EtBr complex was formed by adding 2 μM EtBr to 20 μM CT-DNA. The prepared compound solutions were added to CT-DNA/EtBr solutions in

concentrations from 2.5 μM to 35 μM increasing by 2.5 μM and incubated for 3 hours. Emission spectra ranking between 500–750 nm were recorded in each experiment using 480 nm as the excitation wavelength.

In the obtained emission spectra, the intensities at approximately 600 nm where maximum emission occurred were taken into consideration and the necessary calculations were made using the Stern–Volmer equation below:[28]

$$F_0/F = 1 + K_{sv}[Q]$$

F_0 and F are the fluorescence intensities of the CT-DNA + EtBr complex measured in the absence and presence of the compounds, respectively, K_{sv} is a linear Stern–Volmer quenching constant, and [Q] is the concentration of the compound(s).

According to the results of the experiments with EtBr and compounds **4** and **5**, the emission of the EtBr–DNA complex decreased with the increasing concentration of the compound (Fig. 13a and c). Here, we can say that the compounds bound to CT-DNA, preventing EtBr from binding. The K_{sv} constants calculated using the Stern–Volmer equation were found to be 4.3×10^3 M^{-1} and 5.9×10^3 M^{-1}, respectively (Fig. 13b and d). Both compounds led to a gradual decrease in the emission spectrum and very close K_{sv} values appeared.

Fig. 13e shows that the emission intensity of the EtBr–DNA complex at about 600 nm decreased with the addition of compound **6** at increasing concentrations. The calculated K_{sv} constant was found to be 2.4×10^3 M^{-1} (Fig. 13f). As in compounds **4** and **5**, it can be interpreted that this compound performed intercalative binding with DNA.

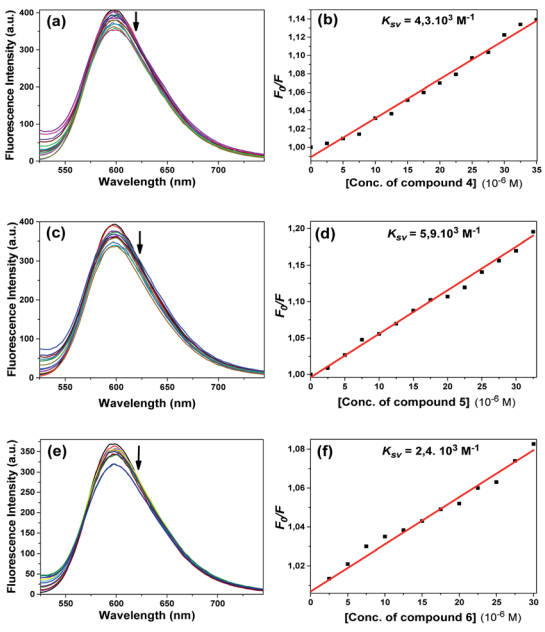

Fig. 13 Fluorescence emission spectra of EtBr bound with CT-DNA ([DNA] = 2.0×10^{-5} M, [EtBr] = 2.0×10^{-6} M) in the absence (black) and presence (other colours) of compounds **4** (a), **5** (c), and **6** (e) in Tris–HCl/NaCl buffer upon addition of CT-DNA and EtBr [from top to bottom (0–35 μM)] with increments of 2.5 μM of the compounds. Arrows represent the changes in the fluorescence intensity upon increasing the compound concentration. For compounds **4** (b), **5** (d) and **6** (f), linear fitting graphs were used to calculate the quenching constant K_{sv} based on the Stern–Volmer equation.

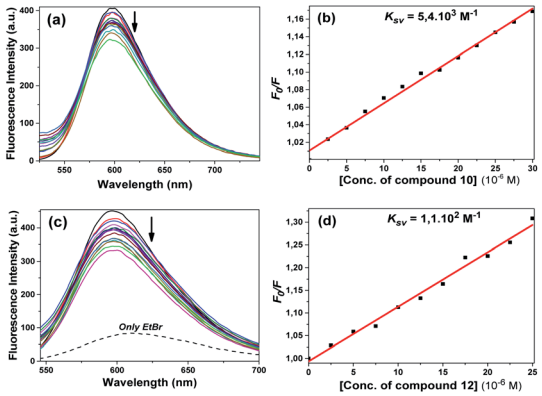

Fig. 14 Fluorescence emission spectra of EtBr bound with CT-DNA ([DNA] = 2.0×10^{-5} M, [EtBr] = 2.0×10^{-6} M) in the absence (black) and presence (other colours) of compounds **10** (a) and **12** (c) in Tris–HCl/NaCl buffer upon the addition of CT-DNA and EtBr [from top to bottom (0–35 μM)] with increments of 2.5 μM of the compounds. Arrows represent the changes in fluorescence intensity upon increasing the compound concentration. For compounds **10** (b) and **12** (d) linear fitting graphs were used to calculate the quenching constant K_{sv} based on the Stern–Volmer equation.

Compounds **10** and **12** had the same effect as the other compounds competitively substituted with EtBr, causing a slight reduction in the emission of the EtBr–DNA complex (Fig. 14a and c). Stern–Volmer quenching constants were also found to be 5.8×10^3 M^{-1} and 1.1×10^2 M^{-1}, respectively (Fig. 14b and d). Unlike other compounds, compound **11** increased the EtBr emission intensity. The obtained emission spectrum is not included here because a different effect occurred. Some studies in the literature have shown that some molecules can bind to the cavity of the DNA by the groove binding mode through hydrophobic interactions, and in this case, the EtBr–DNA complex can cause an increase in the emission intensity.[36] The same effect may apply for compound **11**.

The calculated quenching constants of the compounds using the reductions in the emission intensity of the CT-DNA + EtBr complex are given in Table 2. According to the calculated K_{sv} values, compounds **5** and **10** achieved the strongest binding with CT-DNA, while the compounds following them were **4** > **6** >

Table 2 The calculated quenching constants (K_{sv}) (M^{-1}) and correlation coefficient values (R^2) of the compounds that interact with CT-DNA

Compound	Functional group	K_{sv} (M^{-1})	R^2
4	—	4.3×10^3	0.989
5	Chloro	5.9×10^3	0.989
6	Methyl	2.4×10^3	0.987
10	Benzyl	5.8×10^3	0.997
12	Sulfur(S)	1.1×10^2	0.988

Table 3 The binding free energy scores for the synthesized compounds with DNA

Compound	Binding free energy (kcal mol^{-1})
4	−10.9
5	−15.2
6	−11.4
7	−10.9
10	−20.1
11	−13.5
12	−10.0

12, respectively. Compound **10** had the highest binding constant in fluorescence studies and it gave the same value as compound **5** in competitive displacement studies with EtBr.

Molecular docking studies

To predict the noncovalent binding conformations and affinities of the newly synthesized compounds toward DNA, molecular docking was carried out. The predicted free energy values of binding are given in Table 3. Active compounds **10**, **5**, and inactive compound **12**, were selected for comparison according to the experimental results of their binding strength to DNA. The most energetically profitable poses of **10**, **5** and **12** in the DNA binding site are given in Fig. 15 with both the three-dimensional (3D) structures and the molecular surface representations (Fig. 15a–c) and two-dimensional (2D) interaction diagrams (Fig. 15d–f). Docking figures for the other compounds **4**, **6**, **7** and **11** are presented as ESI (Fig. S5†). As seen in Fig. 15, the interaction of the compounds with the DNA was dominated by noncovalent C–H···π, hydrogen bonding and water-mediated contacts. For the docking of the compounds **10**, **5** and **12** to DNA, binding free energy values of −20.1, −15.2, and −10.0 kcal mol^{-1} were predicted, respectively. Lower binding energy values indicate more preferable bonding interactions between compound–DNA complexes. It was observed that compound **12** with the highest binding energy, interacts less with DNA than other compounds. Five- and six-membered rings of benzothiazole groups of 12 interacted with the DNA residues A17 and A18 *via* C–H···π interactions. In the case of compound **10**, it was predicted that there were many more C–H···π interaction networks with DNA residues as compared to **12**: two between the toluene ring bound to benzimidazole group and DNA residues C11 and A17, five- and six-membered rings of other benzimidazole groups and G12, the ring of the *tert*-butyl methoxybenzene group of **10** and the G16 residue. For the docking of compound **5**, hydrogen bonding and O–H···π interactions as well as C–H···π interactions with G12, T19, A18 residues, and water molecules were observed.

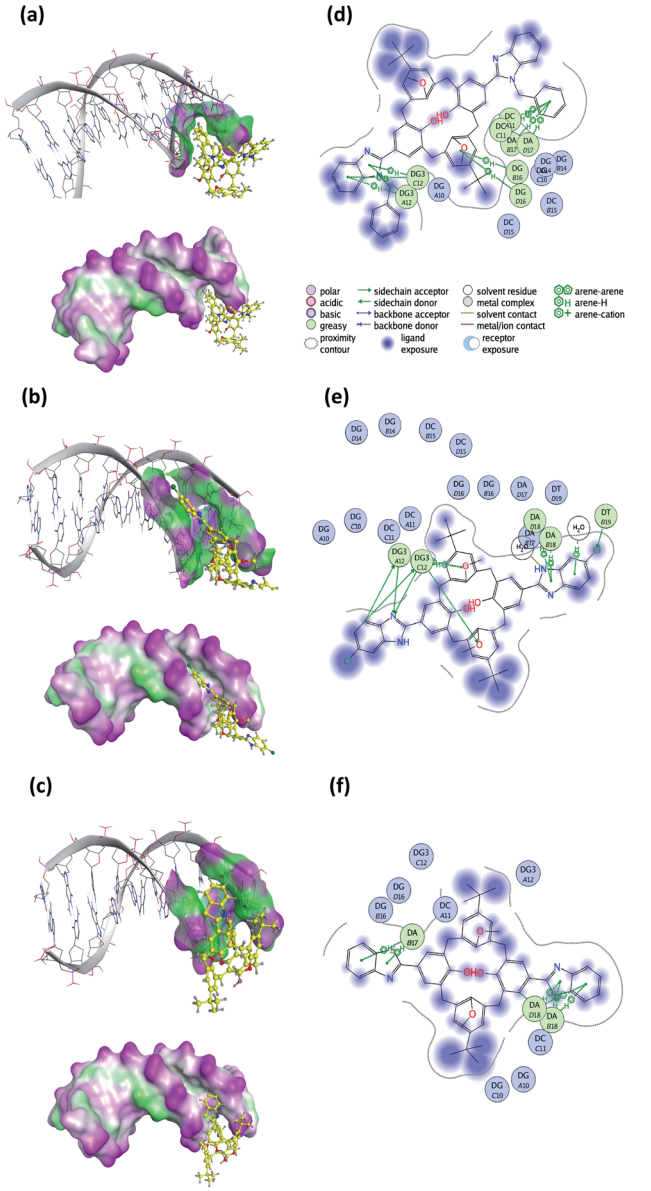

Fig. 15 Three-dimensional (3D) docked structures with molecular surface representations (left column) and two-dimensional (2D) interaction plots (right column) obtained for the most energetically profitable poses of the compound–DNA complexes: (a) and (d) compound **10**; (b) and (e) compound **5**; (c) and (f) compound **12** (PDB ID: 1BNA).

Experimental

Reagents and techniques

Chemicals and solvents were obtained from commercial sources (Merck and Sigma) and were used without further purification. DNA (supercoiled pBR322) and restriction enzymes (*BamHI* and *HindIII*) were purchased from Thermo-Fischer Scientific. Calf thymus DNA was supplied by Sigma. Measurements of ^{1}H NMR and ^{13}C NMR spectra were recorded in $CDCl_3$ and DMSO-d_6 on a Varian MR 400 MHz spectrometer using TMS as an internal standard. A Perkin Elmer 100 FTIR spectrophotometer was used to record the infrared spectra of all compounds (4000–400 cm^{-1}). Mass spectra were obtained using a Bruker Microflex LT MALDI-TOF mass spectrometer. Elemental analyses (C, H, and N) were performed using a Leco 932 CHNS analyzer. The UV-vis. measurements were performed

on a Shimadzu UV 1800 UV-vis spectrometer. A Perkin Elmer LS 55 Fluorimeter was used for fluorescence spectra. Microwave irradiated reactions were performed using a CEM MDS-2000, and a household microwave oven. The determination of the melting points was performed using a Büchi B-540 instrument. Analytical TLC was performed on precoated silica gel plates (SiO_2, Merck PF254). All aqueous solutions were prepared with purified water or ultrapure water purified by a Millipore Milli-Q Plus water purification device.

Synthetic procedures

The *p-tert*-butylcalix[4]arene **1** and its derivatives **2** and **3**, and **8** and **9** were synthesized according to the literature procedures.[22–25]

Synthesis of compound 4. Here, 0.62 g (1 mmol) of compound **3** and 1.08 g (10 mmol) of *o*-phenylenediamine were weighed and 0.83 g (5 mmol) of potassium chloride (KI) was added. Then, 50 mL of dimethylformamide (DMF) was added and refluxed in a laboratory-type microwave device for about 3 hours, or 2 minutes in the domestic microwave oven, and then heated to 80 °C for 48 hours. To the cooled mixture was added 50 mL of ethyl acetate and water. The mixture was taken into the separating funnel, shaken and allowed to separate. The final product formed on the interface was obtained and purified from ethanol. Compound **4** was obtained in 35% yield. Mp 284–286 °C. FTIR: 1620 cm^{-1} (C=N). ^{1}H NMR (DMSO-d_6): δ ppm 1.05 (s, 18H, Bu^t), 3.57 (d, J = 13.1 Hz, 4H, $ArCH_2Ar$), 3.94 (s, 6H, OCH_3), 4.24 (d, J = 13.1 Hz, 4H, $ArCH_2Ar$), 7.12 (bs, 8H, Calix. ArH, Benzim. ArH), 7.54 (dd, J = 7.04 Hz, 4H, Benzim. ArH), 8.05 (s, 4H, Calix. ArH), 8.74 (s, 2H, OH), 12.54 (s, 2H, Benzim. NH). ^{13}C NMR (DMSO-d_6): δ ppm 155, 153.2, 152.2, 151.7, 150.5, 147.7, 132.4, 130.7, 128.8, 127.5, 126.4, 123.7, 121.9, 121.6, 117.7, 64.0, 34.5, 31.6, 31.5. MALDI-TOF MS: (CHNO = 796.4 m/z) 796.12 [M^+] (Fig. S1†). Anal. cal. for $C_{52}H_{52}N_4O_4$: C, 78.36; H, 6.58; N, 7.03%. Found: C, 78.0; H, 6.8; N, 7.1%.

General procedure for synthesis of compounds 5–7 and 10, 11

Here, 0.5 g (0.805 mmol) of the dialdehyde compound (**3**), 1.691 mmol of *o*-phenylenediamine derivatives [4-methyl-*o*-phenylenediamine (0.21 g), 4-nitro-*o*-phenylenediamine (0.26 g), and 4-chloro-*o*-phenylenediamine (0.24 g), *N*-benzyl-*o*-phenylenediamine (0.34 g), and *N*-*p*-nitrobenzyl-*o*-phenylenediamine (0.41 g), respectively] were weighed. Then, 0.28 g (1.691 mmol) of KI was added, followed by 50 mL of DMF, and kept in the household microwave device for approximately 1–2 min. After being removed from the device and cooled slightly, it was heated to 80 °C by connecting it back to the condenser for 24–96 hours (96 hours for **5**, **10** and **11**, 72 hours for **6** and 24–48 hours for **7**). It was cooled when the reaction was determined to be over by TLC and FTIR. To the mixture was added 50 mL of ethyl acetate and water. The mixture was taken into the separating funnel, shaken and allowed to separate. The ethyl acetate phase was obtained, dried with $CaCl_2$, then the solvent was removed and washed with ethanol.

Compound 5. Compound **5** was obtained in 40% yield. Mp >300 °C (decomposition). FTIR: 1664, 1621 cm^{-1} (C=N). ^{1}H NMR (DMSO-d_6): δ ppm 1.07 (s, 18H, Bu^t), 3.61 (d, J = 12.8 Hz, 4H, $ArCH_2Ar$), 3.97 (s, 6H, OCH_3), 4.27 (d, J = 12.8 Hz, 4H, $ArCH_2Ar$), 7.07–7.29 (overlapped, 6H, Calix. ArH), 7.43–7.72 (m, 4H, Calix. ArH, Benz. ArH), 8.05 (s, 4H, Benzyl. ArH), 8.81 (s, 2H, OH), 12.76 (s, 2H, Benzyl. NH). ^{13}C NMR (DMSO-d_6): δ ppm 155.3, 147.7, 145.4, 142.7, 135.1, 134.8, 132.3, 132.1, 128.8, 128, 127.7, 126.5, 125.3, 124.7, 118.1, 64.0, 34.5, 31.6, 31.5. MALDI-TOF MS: (CHClNO = 864.32 m/z) 864.57 [M^+] (Fig. S1†). Anal. calc. for $C_{52}H_{50}Cl_2N_4O_4$: C, 72.1; H, 5.82; N, 6.47%. Found: C, 71.6; H, 6.2; N, 5.9%.

Compound 6. Compound **6** was obtained in 45% yield. Mp 259–261 °C. FTIR: 1664, 1628 cm^{-1} (C=N). ^{1}H NMR (DMSO-d_6): δ ppm 1.08 (s, 18H, Bu^t), 2.46 (s, 6H, $ArCH_3$), 3.60 (d, J = 12.8 Hz, 4H, $ArCH_2Ar$), 3.97 (s, 6H, OCH_3), 4.28 (d, J = 12.8 Hz, 4H, $ArCH_2Ar$), 6.99 (d, J = 8.2 Hz, 2H, Benzyl. ArH), 7.15 (s, 4H, Calix. ArH), 7.35 (s, 2H, Benz. ArH), 7.44 (d, J = 8.2 Hz, 2H, Benzyl. ArH), 7.77–8.19 (m, 5H, Calix. ArH, OH), 8.77 (s, 1H, OH), 12.8 (bs, 2H, Benz) NH. ^{13}C NMR (DMSO-d_6): δ ppm 154.9, 151.8, 151.7, 147.7, 132.4, 132.1, 131.3, 130.8, 129.3, 128.8, 127.4, 126.5, 126.4, 123.5, 121.5, 64, 34.5, 31.5, 31.4, 21.8. MALDI-TOF MS: (CHNO = 824.43 m/z) 824.07 [M^+] (Fig. S2†). Anal. Cal. for $C_{54}H_{56}N_4O_4$: C, 78.6; H, 6.84; N, 6.79%. Found: C, 77.6; H, 7.2; N, 6.5%.

Compound 7. Compound **7** was obtained in 25% yield. Mp 275–277 °C. FTIR: 1624 cm^{-1} (C=N), 1521 cm^{-1} (NO_2). ^{1}H NMR (DMSO-d_6): δ ppm 1.09 (bs, 18H, Bu^t), 3.60 (d, J = 13.1 Hz, 4H, $ArCH_2Ar$), 3.96 (bs, 6H, OCH_3), 4.26 (d, J = 13.1 Hz, 4H, $ArCH_2Ar$), 6.64–6.81 (m, 4H, Calix. ArH), 7.07–7.37 (m, 4H, Calix. ArH), 7.85–7.93 (m, 4H, Benzyl. ArH), 8.04–8.21 (bs, 2H, Benz. ArH), 8.59 (s, 1H, OH), 9.04 (s, 1H, OH), 13.32 (s, 2H, Benzyl. NH). ^{13}C NMR (DMSO-d_6): δ ppm 159.6, 156.6, 151.6, 151.3, 147.9, 147.7, 136.5, 135.0, 132.8, 130.5, 129.2, 128.3, 126.5, 124.2, 112.8, 64, 34, 31.5, 31.3. MALDI-TOF MS: (CHNO = 886.37 m/z) 886.60 [M^+] (Fig. S2†). Anal. cal. for $C_{52}H_{50}N_4O_4$: C, 70.4; H, 5.68; N, 9.47%. Found: C, 70.6; H, 6.2; N, 9.5%.

Compound 10. Compound **10** was obtained in 35% yield. Mp 190–192 °C. FTIR: 1624 cm^{-1} (C=N). ^{1}H NMR (DMSO-d_6): δ ppm 1.08 (s, 18H, Bu^t), 3.61 (d, J = 13.5 Hz, 4H, $ArCH_2Ar$), 3.95 (bs, 6H, OCH_3), 4.10–4.45 (m, 4H, $ArCH_2Ar$), 5.31 (s, 4H, NCH_2), 6.73–7.37 (m, 12H, Calix. ArH, ArH), 7.37–7.78 (m, 6H, Calix. ArH, ArH), 7.79–8.17 (m, 5H, ArH) 8.18–8.45 (m, 2H, ArH), 8.55 (s, 1H, ArH), 8.82 (s, 2H, ArOH). MALDI-TOF MS: (CHNO = 976.49 m/z) 976.04 [M^+] (Fig. S3†). Anal. cal. for $C_{66}H_{64}N_4O_4$: C, 81.1; H, 6.60; N, 5.73%. Found: C, 80.6; H, 6.8; N, 5.6%.

Compound 11. Compound **11** was obtained in 45% yield. Mp 259–262 °C. FTIR: 1624 cm^{-1} (C=N), 1519 cm^{-1} (NO_2). ^{1}H NMR (DMSO-d_6): δ ppm 0.96 (s, 18H, Bu^t), 3.51 (d, J = 13.0 Hz, 4H, $ArCH_2Ar$), 3.91 (bs, 6H, OCH_3), 4.18 (d, J = 13.0 Hz, 4H, $ArCH_2Ar$), 5.71 (s, 4H, NCH_2), 6.89 (m, 2H, Calix. ArH), 7.03–7.50 (m, 11H, Calix. ArH, ArH), 7.50–7.89 (m, 6H, ArH), 7.97–8.06 (m, 1H, ArH), 8.16 (d, J = 8.61 Hz, 4H, ArH), 8.30–8.47 (m, 1H, ArOH), 8.55–8.77 (m, 1H, ArOH). ^{13}C NMR (DMSO-d_6): δ ppm 159.2, 154.9, 154.1, 151.6, 147.3, 145.3, 143.2, 136, 132.2, 131.3, 130.8, 129.9, 128.9, 127.8, 126.4, 124.4, 122.7, 119.5, 111.2, 63.9, 47.7, 34.3, 34.1, 31.3. MALDI-TOF MS: (CHNO = 1066.46 m/z) 1066.05 [M^+] (Fig. S3†). Anal. cal. for $C_{66}H_{62}N_6O_8$: C, 74.3; H, 5.86; N, 7.87%. Found: C, 74.6; H, 6.0; N, 7.7%.

Synthesis of compound 12

Here, 0.62 g (1 mmol) of compound **3** was weighed and 1.068 mL (10 mmol) of 2-aminothiophenol and 0.83 g (5 mmol) of KI were added. Next, 50 mL of DMF was added and refluxed for 2–3 hours in a laboratory microwave. To the cooled mixture was added 50 mL of ethylacetate and water. The mixture was taken into the separating funnel, shaken and allowed to separate. The ethyl acetate phase was separated off, dried with $MgSO_4$, and the solvent removed and purified from hot ethanol. Compound **12** was obtained in 55% yield. Mp 258–262 °C FTIR: 1658 cm^{-1} (C=N), 1373 cm^{-1} (C–S). ^{1}H NMR ($CDCl_3$): δ ppm 0.99 (s, 18H, Bu^t), 3.57 (d, $J = 13.3$ Hz, 4H, $ArCH_2Ar$), 4.03 (s, 6H, OCH_3), 4.36 (d, $J = 13.3$ Hz, 4H, $ArCH_2Ar$), 6.60 (bs, 1H, Calix. ArH), 6.72 (bs, 1H, Calix. ArH), 6.84 (s, 1H, Calix. ArH), 6.94 (s, 2H, Calix. ArH), 7.18 (d, $J = 6.5$ Hz, 2H, Thia. ArH), 7.35 (t, $J = 6.5$ Hz, 2H, Thia. ArH), 7.48 (t, $J = 6.5$ Hz, 2H, Thia. ArH), 7.69 (s, 1H, Calix. ArH), 7.82–7.90 (m, 4H, Calix. ArH, ArOH), 8.04–8.08 (m, 2H, Thia. ArH). ^{13}C NMR ($CDCl_3$): δ ppm 156.2, 154.3, 151.3, 148.6, 148, 137, 136.8, 134.8, 131.6, 129.1, 127.8, 125.9, 122.5, 121.4, 118.3, 63.6, 34.1, 31.2, 31.1. MALDI-TOF MS: (CHNOS = 830.32 *m/z*) 830.70 [M^+] (Fig. S4†). Anal. cal. for $C_{52}H_{50}N_2O_4S_2$: C, 75.15; H, 6.06; N, 3.37; S, 7.72%. Found: C, 74.8; H, 6.2; N, 3.4; S, 7.80%.

DNA studies

pBR322 plasmid DNA studies. For these studies, each material and prepared buffer solution was autoclaved and sterilized before use. pBR322 plasmid DNA was prepared as a 0.5 μg mL^{-1} plasmid DNA solution with buffer prepared as 10 mM Tris–HCl and 1 mM EDTA at pH 7.4. The compounds were prepared as stock in DMF at 10 000 MM. The buffer solution prepared for both DMF and DNA was used in half-dilution processes (5000, 2500, 1250, 625 μM). The prepared stock DNA solution contained 0.5 μg mL^{-1} plasmid DNA for each substance (30 μL samples) and was incubated in the dark in a water bath at 37 °C for 24 hours. At the end of this period, 10 μL samples were taken from each sample and mixed with 3 μL of dye and loaded onto 1% agarose gel [prepared with 1XTAE (Tris + acetic acid + EDTA)] and electrophoresed in 1XTAE buffer at 60 V for 2 or 3 hours. At the end of this time, the gel was removed and 10 μL of 0.5 mg mL^{-1} (100 μM) EtBr solution was shaken for 30 minutes, after which the images of the gels were recorded under a UV lamp. In experiments with restriction enzymes, 8 μL samples were taken from samples incubated overnight for both *BamHI* and *HindIII*. Then, 1 unit of enzyme (0.1 μL) and buffer (1 μL) was added to these samples and incubated for one hour at 37 °C in a hot water bath. At the end of this period, the samples were removed from the hot water bath and immediately transferred to an ice bath. The same operations described above were performed and the images were recorded.

CT-DNA studies. CT-DNA was dissolved in 10 mM Tris–HCl + 50 mM NaCl pH 7.2 buffer solution. It was kept at 4 °C for 1–2 days at equilibrium. At the end of this period, the DNA was taken and its absorbances at 260 nm and 280 nm were measured and a stock solution was prepared according to the A_{260}/A_{280} ratio between 1.8–1.9, showing that the DNA was sufficiently transformed into the free form.[30] Taking into account the absorbance at 260 nm, the ε (molar absorption coefficient) value of 6600 M^{-1} cm^{-1} was determined. The compounds were prepared by dissolving in 0.125 mM stock solutions in DMF. The proportion of DMF in the measured solution was kept at 2%. This ratio was used because smaller amounts of the materials precipitated. The volumes were completed by adding a buffer solution (10 mM Tris–HCl + 50 mM NaCl pH 7.2) to a final volume of 3 mL. The prepared samples were incubated at room temperature and in the dark for 24 hours. Fluorescence spectrophotometer measurements were performed in a 3 mL cuvette. UV-vis spectrophotometer measurements were made using the same samples as in fluorescence spectroscopy. In EtBr studies, EtBr was dissolved with the same buffer solution and prepared freshly for each measurement. Samples prepared with EtBr were incubated for 3 hours at room temperature and in the dark.

Molecular docking computations

Before the molecular docking, the geometries of the initial structures of the ligands considered were optimized by using the Gaussian 09 software[33] with the semi-empirical parametric method 6 (PM6).[34] The crystal structure of the DNA dodecamer was retrieved from the RCSB Protein Data Bank (http://www.rcsb.org/pdb/), under the accession code 1BNA.[28b] Molecular Operating Environment (MOE) software[35] was used for molecular docking studies. The co-crystallized water molecules farther than 4.5 Å from ligand or DNA were deleted from the crystal structure. DNA–ligand complexes were energy-minimized to a gradient of 0.01 kcal (mol^{-1} $Å^{-1}$), and protonated by the force field AMBER99. Charges on the DNA and ligands were assigned using the force fields AMBER99 and MMF94X, correspondingly. Possible ligand-binding sites were identified by the "Site Finder" module of the MOE. The Triangle Matcher Algorithm and scoring functions of London dG and GBVI/WSA dG were used to produce 30 poses of each ligand. All poses generated with docking were analyzed and the best-scored pose with the lowest binding energy and root mean square value for each compound was selected for further investigation of interactions with the DNA.

Conclusions

In this study, the synthesis and characterization of six different *p*-benzimidazole-derived and a benzothiazole-derived *p-tert*-butylcalix[4]arene compounds were performed and the interactions of the compounds obtained with pBR322 plasmid DNA and CT-DNA were evaluated by various methods. Compounds showing cleavage effects on pBR322 plasmid DNA were **6** and **10** (at the highest concentration, 10 000 μM), while other compounds **5**, **7**, **11** and **12** caused different changes in the structure of the plasmid DNA. CT-DNA interaction experiments were evaluated using UV-vis and molecular fluorescence spectral studies. The results obtained from UV-vis studies showed that there was a hyperchromic effect, proving that all of the

compounds, except compound **7**, interact with DNA. The stoichiometries of the binding modes of the compounds with DNA and the evaluation of the interaction strengths of the complexes formed were performed by fluorescence spectroscopy. The first of these studies showed that the emission intensities of compounds **4** and **5** were increased by the addition of DNA, whereas those of compounds **10–12** decreased. DNA binding constants (K_b) and the number of molecules that bind to DNA were calculated for the compounds giving both conditions. Compounds **7** and **10** had the highest K_b constants (9.3×10^2 M^{-1} and 7.1×10^3 M^{-1}, respectively). In the displacement experiments performed with EtBr, results in line with previous studies were obtained. Compounds **5** and **10** had the highest K_{sv} constants (5.9×10^3 M^{-1} and 5.8×10^3 M^{-1}, respectively). Consequently, when the obtained results were combined, it was evaluated that the compounds showed binding strengths toward CT-DNA of the order of **10** > **5** > **4** > **11** > **6** > **12**.

Docking of the synthesized compounds into the DNA binding site was carried out. Docking results complemented well the experimental results on binding strength of the compounds to DNA. Lower binding free energies and much more interaction networks were observed for compounds that more strongly interacted with the DNA than weaker ones. For the docking of compounds **10**, **5** and **12**, the DNA residues C11, G12, G16, A17, A18 and T19 played a major role in the binding site.

Experimental results have shown that the benzyl ring of compound **10** is more potent between the nucleotides of DNA than other compounds because of its aromatic and planar structure. In a similar study, it was determined that the benzimidazole compounds with substituted benzyl groups are effective on CT-DNA.[36] Compound **11**, unlike **10**, has a nitro group attached to the benzyl ring. However, the fact that compound **7** with the nitro group had no activity toward the CT-DNA led to the idea that it was due to the structure of the nitro group. We, therefore, thought that compound **11** did not show activity as compound **10**. Secondly, compound **5**, which strongly binds to DNA, has the chloro-group; chlorine, an electronegative atom, increased its ability to bind to the DNA. It has been reported that compounds containing halogens show activity toward DNA.[30,31] Compound **4** is a calixarene compound without a substituent attached to the ring and its binding to DNA was stronger than the remaining compounds. Compounds **10** and **5** took first place in the ranking according to the calculated K_b and K_{sv} constants. Finally, when comparing studies with benzothiazole compound (**12**), it was concluded that benzimidazole compounds bind more strongly with CT-DNA than a benzothiazole compound.

Some of the compounds synthesized in this study showed activity against bacterial plasmid DNA, some against CT-DNA and some against both DNA types. While compounds **4–6**, and **10** were found to bind to DNA in the intercalative mode, compound **11** was also bound to DNA, possibly with the groove binding mode.

The development of new and effective drugs has become essential and important due to antibiotic resistance, which is a major problem in our age that has become more and more scary day by day. For this reason, the design and synthesis of new compounds with antibacterial properties have been among the subjects that scientists have worked hard on. For this purpose, it was seen in this study that two of the synthesized compounds could break down the plasmid DNA, which is the protective DNA of bacteria.

On the other hand, the absence of the drug(s) that completely cure cancer, one of the biggest health problems of today, requires the synthesis of new and effective molecules. For this purpose, the studies carried out with CT-DNA are preliminary studies and the active compounds can be used in future experimental *in vitro* anticancer studies.[12,16,30,32,37–39]

Conflicts of interest

There are no conflicts to declare.

Acknowledgements

We would like to thank the Research Foundation of Selcuk University, Konya Turkey [grant number BAP 2017/17201115] for its financial support of this work produced from a part of Ş. Ç. Özkan's PhD thesis. In addition, the author would like to thank the Department of Chemistry of Gebze Technical University for its laboratory and device facilities.

Notes and references

1 (*a*) A. Villiers, *C. R. Acad. Sci.*, 1891, 536–538; (*b*) F. Schardinger and Z. Unters, *Nahr. Genussm.*, 1903, **6**, 865–880.

2 (*a*) C. J. Pedersen, *J. Am. Chem. Soc.*, 1967, **89**(26), 7017–7036; (*b*) C. J. Pedersen, *J. Am. Chem. Soc.*, 1967, **89**(10), 2495–2496.

3 C. D. Gutsche, *Calixarenes; Monographs in Supramolecular Chemistry*, ed. J. F. Stoddart, The Royal Society of Chemistry, Cambridge, 1989, p. 1.

4 (*a*) D. Baurer, M. Blumberg, M. Köckerling and C. Mamat, *RSC Adv.*, 2019, **9**, 32357–32366; (*b*) J. Rodríguez-Lavado, A. Lorente, E. Flores, A. Ochoa, F. Godoy, P. Jaque and C. Saitz, *RSC Adv.*, 2020, **10**, 21963–21973; (*c*) M. Phichi, A. Imyim, T. Tuntulani and W. Aeungmaitrepirom, *Anal. Chim. Acta*, 2020, **1104**, 147–155.

5 (*a*) B. Mokhtari and K. Pourabdollah, *Asian J. Chem.*, 2013, **25**(1), 1–12; (*b*) F. K.-W. Hau, H.-S. Lo and V. W.-W. Yam, *Chem.–Eur. J.*, 2016, **22**, 3738–3749; (*c*) S. Erdemir, B. Tabakci and M. Tabakci, *Sens. Actuators, B*, 2016, **228**, 109–116.

6 (*a*) M. Kandpal, A. K. Bandela, V. K. Hinge, V. R. Rao and C. P. Rao, *ACS Appl. Mater. Interfaces*, 2013, **5**, 13448–13456; (*b*) Z. Zheng, W.-C. Geng, J. Gao, Y.-J. Mu and D.-S. Guo, *Org. Chem. Front.*, 2018, **5**, 2685–2691; (*c*) H. Kaur, N. Singh, N. Kaur and D. O. Jang, *Sensor. Actuator. B Chem.*, 2019, **284**, 193–201.

7 (*a*) M. Mourer, R. E. Duval, P. Constant, M. Daffé and J.-B. Regnouf-de-Vains, *ChemBioChem*, 2019, **20**, 911–921; (*b*) Ş. Ç. Özkan, A. Yılmaz, E. Arslan, L. Açık, Ü. Sayın and E. Gülbahçe Mutlu, *Supramol. Chem.*, 2015, **27**, 255–267.

8 (*a*) M. N. Soares Jr, T. M. Gáscon, F. L. A. Fonseca, K. S. Ferreira and I. A. Bagatin, *Mater. Sci. Eng. C*, 2014, **40**, 260–266; (*b*) Z. D. Gezelbash and K. A. Dilmaghani, *J. Chin. Chem. Soc.*, 2020, **67**, 1446–1452.

9 Y. Tauran, J. P. Cerón-Carrasco, M. Rhimi, F. Perret, B. Kim, D. Collard, A. W. Coleman and H. Pérez-Sánchez, *Antibiotics*, 2019, **8**(73), 1–15.

10 (*a*) M. Mourer, N. Psychogios, G. Laumond, A.-M. Aubertin and J.-B. Regnouf-de-Vains, *Bioorg. Med. Chem.*, 2010, **18**, 36–45; (*b*) F. N. Pur, *Mol. Divers.*, 2020, DOI: 10.1007/s11030-020-10042-0.

11 G. Granata, I. Paterniti, C. Geraci, F. Cunsolo, E. Esposito, M. Cordaro, A. R. Blanco, S. Cuzzocrea and G. M. L. Consoli, *Mol. Pharm.*, 2017, **14**(5), 1610–1622.

12 (*a*) R. P. M. Dings, J. I. Levine, S. G. Brown, L. Astorgues-Xerri, J. R. MacDonald, T. R. Hoye, E. Raymond and K. H. Mayo, *Invest. New Drugs*, 2013, **31**, 1142–1150; (*b*) B. Yilmaz, A. T. Bayac and M. Bayrakci, *Appl. Biochem. Biotechnol.*, 2020, **190**, 1484–1497; (*c*) L. An, C. Wang, L. Han, J. Liu, T. Huang, Y. Zheng, C. Yan and J. Sun, *Front. Chem.*, 2019, **7**, 856; (*d*) M. Oguz, A. Gul, S. Karakurt and M. Yilmaz, *Bioorg. Chem.*, 2020, **94**(1–8), 103207; (*e*) E. B. Noruzi, B. Shaabani, S. Geremia, N. Hickey, P. Nitti and H. S. Kafil, *Molecules*, 2020, **25**(1–19), 370.

13 (*a*) S. B. Nimse and T. Kim, *Chem. Soc. Rev.*, 2013, **42**, 366–386; (*b*) Y. Tauran, M. Kumemura, M. C. Tarhan, G. Perret, F. Perret, L. Jalabert, D. Collard, H. Fujita and A. W. Coleman, *Sci. Rep.*, 2019, **9**(1–13), 5816; (*c*) M. Oguz, E. Kalay, S. Akocak, A. Nocentini, N. Lolak, M. Boga, M. Yilmaz and C. T. Supuran, *J. Enzyme Inhib. Med. Chem.*, 2020, **35**(1), 1215–1223.

14 (*a*) F. J. Ostos, J. A. Lebrón, M. L. Moyá, M. Deasy and P. López-Cornejo, *Colloids Surf., B*, 2015, **127**, 65–72; (*b*) R. V. Rodik, A.-S. Anthony, V. I. Kalchenko, Y. Mély and A. S. Klymchenko, *New J. Chem.*, 2015, **39**, 1654–1664.

15 (*a*) Ş. Ç. Özkan, A. Yılmaz and İ. Özmen, *Supramol. Chem.*, 2014, **26**, 25–31; (*b*) K. Samanta, D. S. Ranade, A. Upadhyay, P. P. Kulkarni and C. P. Rao, *ACS Appl. Mater. Interfaces*, 2017, **9**(6), 5109–5117; (*c*) R. Salvio, S. Volpi, T. Folcarelli, A. Casnati and R. Cacciapaglia, *Org. Biomol. Chem.*, 2019, **17**, 7482–7492.

16 (*a*) M. Mirza-Aghayan, M. Yarmohammadi, R. Zadmard and R. Boukherroub, *Supramol. Chem.*, 2014, **26**(5–6), 442–449; (*b*) F. J. Ostos, J. A. Lebrón, P. López-Cornejo, M. López-López, M. García-Calderón, C. B. García-Calderón, I. V. Rosado, V. I. Kalchenko, R. V. Rodik and M. L. Moyá, *J. Mol. Liq.*, 2020, **304**(1–14), 112724.

17 Salahuddin, M. Shaharyar and A. Mazumder, *Arabian J. Chem.*, 2017, **10**, 157–173.

18 H. M. Refaat, *Eur. J. Med. Chem.*, 2010, **45**, 2949–2956.

19 (*a*) S. U. Rehman, T. Sarwar, M. A. Husain, H. M. Ishqi and M. Tabish, *Arch. Biochem.*, 2015, **576**, 49–60; (*b*) X. L. Li, Y. J. Hu, H. Wang, B. Q. Yu and H. L. Yue, *Biomacromolecules*, 2012, **13**, 873–880; (*c*) W. D. Sasikala and A. Mukherjee, *J. Phys. Chem. B*, 2012, **116**, 12208–12212.

20 (*a*) A. Mukherjee, R. Lavery, B. Bagchi and J. T. Hynes, *J. Am. Chem. Soc.*, 2008, **130**, 9747–9755; (*b*) B. A. D. Neto and A. A. M. Lapis, *Molecules*, 2009, **14**, 1725–1746.

21 S. Kunzelmann, C. Morris, A. P. Chavda, J. F. Eccleston and M. R. Webb, *Biochemistry*, 2010, **49**(5), 843–852.

22 C. D. Gutsche, M. Iqbal and D. Stewart, *J. Org. Chem.*, 1986, **51**, 742–745.

23 A. Casnati, A. Arduini, E. Ghidini, A. Pochini and R. Ungaro, *Tetrahedron*, 1991, **47**, 2221–2228.

24 A. Sap, B. Tabakci and A. Yilmaz, *Tetrahedron*, 2012, **68**, 8739–8745.

25 (*a*) The commercial product; (*b*) A. E. Sparke, C. M. Fisher, R. E. Mewis and S. J. Archibald, *Tetrahedron Lett.*, 2010, **51**, 4723–4726.

26 A. Zianna, G. Psomas, A. Hatzidimitriou and M. Lalia-Kantouri, *J. Inorg. Biochem.*, 2016, **163**, 131–142.

27 (*a*) A. Haleel, D. Mahendiran, V. Veena, N. Sakthivel and A. Kalilur Rahiman, *Mater. Sci. Eng. C*, 2016, **68**, 366–382; (*b*) P. Gurumoorthy, D. Mahendiran and A. Kalilur Rahiman, *Chem. Biol. Interact.*, 2016, **248**, 21–35; (*c*) F. Arjmand, S. Parveen, M. Afzal and M. Shahid, *J. Photochem. Photobiol., B*, 2012, **114**, 15–26.

28 (*a*) J. R. Albani, *Principles and Applications of Fluorescence Spectroscopy*, Wiley-Blackwell, Hoboken, 2007; (*b*) M. M. Silva, F. C. Savariz, E. F. Silva-Júnior, T. M. de Aquino, M. H. Sarragiotto, J. C. C. Santos and I. M. Figueiredo, *J. Braz. Chem. Soc.*, 2016, **27**(9), 1558–1568.

29 (*a*) J. R. Lakowicz and G. Weber, *Biochemistry*, 1973, **12**, 4161–4170; (*b*) G. A. Jeffrey, *An Introduction to Hydrogen Bonding*, Oxford University Press, Oxford, 1997; (*c*) S. Scheiner, *Hydrogen Bonding, A Theoretical Perspective*, Oxford University Press, Oxford, 1997.

30 M. Sirajuddin, S. Ali and A. Badshah, *J. Photochem. Photobiol., B*, 2013, **124**, 1–19.

31 M. Ariyaeifar, H. A. Rudbari, M. Sahihi, Z. Kazemi, A. A. Kajani, H. Zali-Boeini, N. Kordestani, G. Bruno and S. Gharaghani, *J. Mol. Struct.*, 2018, **1161**, 497–511.

32 W. Hu, C. Blecking, M. Kralj, L. Šuman, I. Piantanida and T. Schrader, *Chem.–Eur. J.*, 2012, **18**(12), 3589–3597.

33 M. J. Frisch, G. W. Trucks, H. B. Schlegel, G. E. Scuseria, M. A. Robb, J. R. Cheeseman, G. Scalmani, V. Barone, B. Mennucci, G. A. Petersson, H. Nakatsuji, M. Caricato, X. Li, H. P. Hratchian, A. F. Izmaylov, J. Bloino, G. Zheng, J. L. Sonnenberg, M. Hada, M. Ehara, K. Toyota, R. Fukuda, J. Hasegawa, M. Ishida, T. Nakajima, Y. Honda, O. Kitao, H. Nakai, T. Vreven, J. A. Montgomery Jr, J. E. Peralta, F. Ogliaro, M. J. Bearpark, J. Heyd, E. N. Brothers, K. N. Kudin, V. N. Staroverov, R. Kobayashi, J. Normand, K. Raghavachari, A. P. Rendell, J. C. Burant, S. S. Iyengar, J. Tomasi, M. Cossi, N. Rega, N. J. Millam, M. Klene, J. E. Knox, J. B. Cross, V. Bakken, C. Adamo, J. Jaramillo, R. Gomperts, R. E. Stratmann, O. Yazyev, A. J. Austin, R. Cammi, C. Pomelli, J. W. Ochterski, R. L. Martin, K. Morokuma, V. G. Zakrzewski, G. A. Voth, P. Salvador, J. J. Dannenberg, S. Dapprich, A. D. Daniels, Ö. Farkas, J. B. Foresman, J. V. Ortiz, J. Cioslowski and

D. J. Fox, *Gaussian 09*, Gaussian Inc., Wallingford, CT, USA, 2009.
34 J. J. P. Stewart, *J. Mol. Model.*, 2007, **13**(12), 1173–1213.
35 Molecular Operating Environment (MOE), C.C.G.I., 1010 Sherbooke St. West, Suite #910, Montreal, QC, Canada, H3A 2R7, 2014.
36 P. Singla, V. Luxami and K. Paul, *J. Photochem. Photobiol., B*, 2017, **168**, 156–164.
37 M. M. Silva, E. O. O. Nascimento, E. F. Silva-Júnior, J. X. de Araújo-Júnior, C. C. Santana, L. A. M. Grillo, R. S. de Oliveira, P. R. R. Costa, C. D. Buarque, J. C. C. Santos and I. M. Figueiredo, *Int. J. Biol. Macromol.*, 2017, **96**, 223–233.
38 W. Zhou, W. Zhang, Y. Peng, Z.-H. Jiang, L. Zhang and Z. Du, *Molecules*, 2020, **25**, 3180–3197.
39 Y.-Y. Qi, Q. Gan, Y.-X. Liu, Y.-H. Xiong, Z.-W. Mao and X.-Y. Le, *Eur. J. Med. Chem.*, 2018, **154**, 220–232.